IOP Publishing Science and Technology of Advanced Materials
Sci. Technol. Adv. Mater. **11** (2010) 044401 (9pp) doi:10.1088/1468-6996/11/4/044401

Synthesis and characterization of Eu^{3+}, Ti^{4+}@ZnO organosols and nanocrystalline c-$ZnTiO_3$ thin films aiming at high transparency and luminescence

Tangi Aubert[1], Fabien Grasset[1], Michel Potel[1], Virginie Nazabal[1], Thierry Cardinal[2], Stanislav Pechev[2], Noriko Saito[3], Naoki Ohashi[3] and Hajime Haneda[3]

[1] Université de Rennes 1, Unité Science Chimiques de Rennes, UMR 6226 CNRS-UR1, Campus de Beaulieu, CS74205, F-35042 Rennes Cedex, France
[2] CNRS, Université de Bordeaux, ICMCB, 87 avenue du Dr A Schweitzer, Pessac, F-33608, France
[3] National Institute for Materials Science, 1-1 Namiki, Tsukuba, Ibaraki 305-0044, Japan

E-mail: grasset@univ-rennes1.fr and HANEDA.Hajime@nims.go.jp

Received 12 April 2010
Accepted for publication 28 July 2010
Published 14 September 2010
Online at stacks.iop.org/STAM/11/044401

Abstract
By exploiting colloidal properties, such as transparency, rheology and versatile chemistry, we propose to synthesize new photonic nanomaterials based on colloidal solutions and thin films. This contribution highlights our efforts to elaborate and to characterize nanostructures based on the ZnO–TiO_2 system. Using a recently developed sol–gel route to synthesize new Ti^{4+}@ZnO organosols, we were able to prepare, at relatively low temperature (400 °C) and short annealing time (15 min), highly transparent, luminescent, nanocrystalline Eu^{3+} doped c-$ZnTiO_3$ thin films. The organosols and thin films were characterized with UV-visible-near infrared absorption, ellipsometry, photoluminescence spectroscopy, dynamic light scattering, x-ray diffraction and scanning electron microscopy.

Keywords: ceramic, nanoscale materials, thin films/nanomaterials synthesis, optical analysis

1. Introduction

Nanomaterials represent a new class of materials with continuously increasing fields of application, such as environment, catalysis, biotechnology, magnetic and optical devices. Particularly, nanocomposites and nanoceramics prepared with the sol–gel technique have generated much research effort in the past 10 years [1, 2]. One of the largest application areas of sol–gel chemistry is coating and preparation of thin films with specific optical properties, such as tunable visible absorption [3] or strong visible emission [4]. Especially, luminescent materials based on rare-earth (RE) elements, also called phosphors, can be found in numerous everyday applications such as cathode ray tubes, projection television, fluorescent tubes and x-ray detectors [4]. For instance, Y_2O_3:Eu^{3+} is the most popular red phosphor for field emission displays [5]. At the same time, much attention has been paid to the synthesis and luminescent properties of Eu^{3+}-doped orthoborate ($REBO_3$) thin films owing to their desirable properties for vacuum ultraviolet phosphors, which are essential for the new plasma display panels (PDPs) [6, 7]. Both high luminescent efficiency and color purity are required for PDP phosphors. Unfortunately, the red emission from $REBO_3$:Eu^{3+} is often weaker than the orange one, leading to a poor chromaticity of the phosphor [8]. Recently, RE-doped 'ZnTiO' matrix has received much attention in

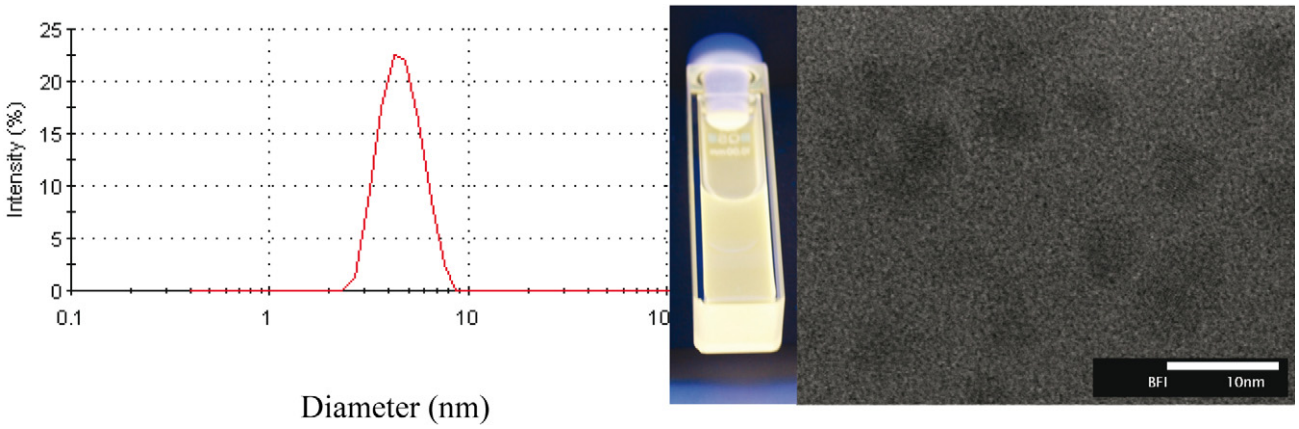

Figure 1. Left: diameter distribution obtained by DLS. Right: image of room-temperature luminescence ($\lambda_{ex} = 365$ nm) and a TEM image of a freshly prepared ZnO organosol.

the sol–gel nanomaterials science for the preparation of luminescent powders [9] or nanocrystalline thin films with high transparency [10]. Two different sol–gel processes have been used. For powders, the nanostructures were prepared by a thermal condensation process employing ethanolic mixtures of zinc acetate dihydrate and titanium alkoxide, and for transparent thin films, the preparation was based on functional ZnO organosols and sol–gel technology [11, 12].

Our contribution to ceramic innovation is based on a sol–gel approach and aims to prepare highly transparent and luminescent Eu^{3+}-doped c-$ZnTiO_3$ thin films. In this work, we focus on the synthesis and the characterization of Eu, Ti@ZnO colloidal organosols.

2. Experimental details

2.1. Synthesis of M@ZnO organosols and thin films

Metal-doped ZnO organosols and thin films were prepared by suspending 0.02 moles of zinc acetate dihydrate (4.39 g) and the appropriate amount of precursor of europium acetate hydrate (up to 10 mol% with respect to Zn content) in 40 ml of n-propanol. The mixture was subsequently distilled on a rotary evaporator, in a preheated silicon oil bath, under ambient atmosphere for 10 min. Nine ml of a methanolic tetramethylammonium-hydroxide stock solution ([TMAH] = 2.37 M) was rapidly added under magnetic stirring to the hot mixture, yielding a turbid precipitate that transformed into a clear concentrated nanocolloid solution after a few minutes. To the fresh sol, we added titanium tetraisopropoxide precursor (Zn/Ti = 1), which readily reacts with the ZnO nanocrystals. After cooling to room temperature, the sol was concentrated on a rotary evaporator (40 °C, 20 torr) to obtain a solution with a concentration up to 1 M. In all cases, the sol was subsequently purified by micropore filtration. Films were deposited on pre-cleaned silica substrates using a dip-coating apparatus and then annealed in air at a temperature between 400 and 800 °C for 15 min. For the temperature-dependent x-ray diffraction (XRD) measurements, the solvent was removed from the xerogel powder using a rotary evaporator (40 °C, 20 torr). The resulting soft gel was kept in an oven at 100 °C for one week for solidification. It was then sintered at a temperature between 400 and 800 °C in air to remove the organic residues and finally transformed into a white powder. Highly pure precursors were used as received. They included zinc acetate dihydrate (Fluka), Europium acetate hydrate (Aldrich), methanolic tetramethylammonium-hydroxide (Fluka), titanium tetraisopropoxide (Fluka) and n-propanol (Fluka).

2.2. X-ray intensity measurements and peak profile analysis

XRD patterns of xerogel nanopowders were recorded at room temperature, in the Bragg–Brentano geometry, using a Bruker D8 diffractometer (40 kV, 30–40 mA, 0.02° angular step and 90 s $step^{-1}$ integration time), Cu$K\alpha_1$ radiation, LynxEye detector and primary monochromators. The data for the thin films were obtained with an Inel CPS 120 curved counter (Cu$K\alpha_1$) at an incident angle of 3°.

2.3. Morphological investigations by SEM and TEM

Scanning electron microscopy (SEM) images were taken with a JEOL JSM 6301F microscope, which incorporates an energy dispersive x-ray spectrometer (EDX), to examine the thickness, microstructure and chemical composition of the films. A transmission electron microscope (TEM) JEOL JEM 2100 FS, equipped with a field emission gun and operating at 200 kV was used to study the ZnO nanoparticles. The samples were prepared by direct deposition of dry powder on carbon-coated Cu grids.

2.4. Dynamic light scattering (DLS) measurements

The mean hydrodynamic diameter ($d(H)$) of the nanocrystals in sols was deduced with DLS measurements. Those were performed with a Zetasizer Nano ZS® from Malvern Instruments using the new non-invasive backscatter technology and detecting scattering at an angle of 173° rather than the conventional 90°. The DLS technique probes the particle diffusion due to Brownian motion and relates it to the particle size. The latter is determined using the

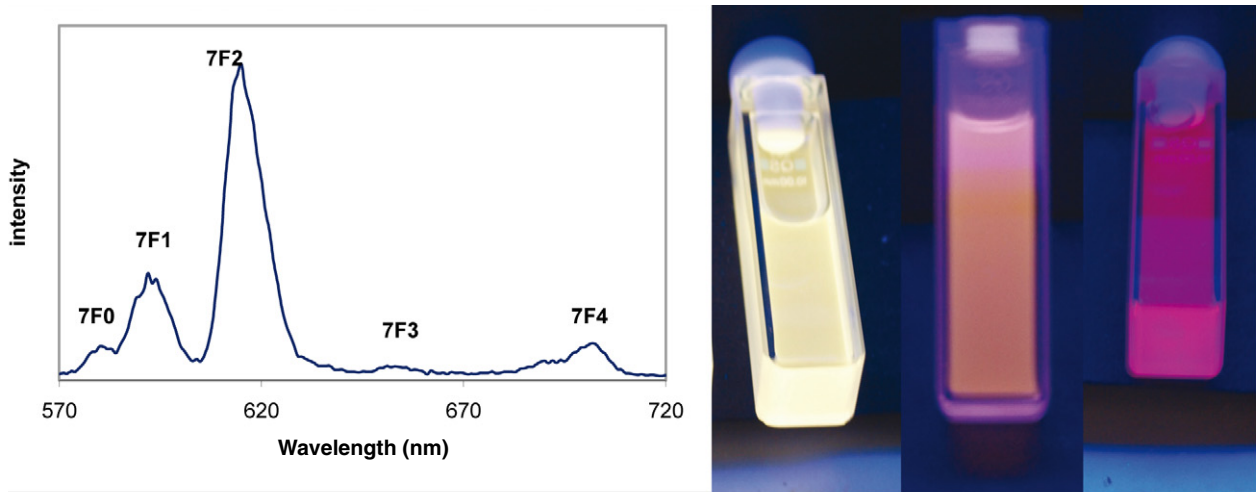

Figure 2. Left: room-temperature luminescence spectrum of Eu^{3+} in sol (a few days old specimen). Right: images of Eu,Ti@ZnO organosol ($\lambda_{ex} = 365$ nm), from left to right—freshly prepared, after 24 h and after a few days.

Stokes–Einstein equation $d(H) = kT/3\pi\eta D$, where D is the translational diffusion coefficient, η is viscosity, k is the Boltzmann constant and T is temperature. The viscosity value in this equation is the dynamic viscosity at zero shear rate; it was measured with an A&D SV10 viscosimeter. Note that the diameter measured by DLS corresponds to the particle diffusion through a fluid and therefore is referred to as the hydrodynamic diameter.

2.5. UV-vis absorption, ellipsometry and photoluminescence spectroscopy

UV-vis and near-infrared absorption spectra of thin films were recorded using a Varian CARY 5 spectrophotometer in the spectral range of 250–2500 nm.

Refractive index was measured with a VASE ellipsometer (J. A. Woollam Co., Inc) equipped with an automatic rotating analyzer. The spectra were typically acquired in the spectral range of 500–2300 nm with the 10 nm step, at an angle of incidence in the range 65–75°. The ellipsometric data in the region of weak absorption were analyzed with a model which includes the substrate and the film having a certain surface roughness (defined using the effective medium approximation). The model uses the Cauchy dispersion formula in the form $n = A + B/\lambda^2 + C/\lambda^4$, where n is refractive index, A, B and C are constants and λ is the wavelength. To improve the agreement between the experimental VASE results and calculated data, a gradient of refractive index in the film was included to the model.

Photoluminescence (PL) spectra were collected with an Edinburgh Instruments FL 900 CDT spectrofluorometer equipped with an M30 monochromator and a photomultiplier tube (R955 Hamamatsu PMT). A 450-W xenon lamp was used as the excitation source. Double monochromators in the excitation and emission parts allow wavelength resolution of 0.05 nm. The spectra were corrected for the intensity and peak position.

The lifetime measurements of the Eu^{3+}:Ti@ZnO gel and xerogel nanopowder were performed with a setup which includes a MicroFlash lamp, monochromators, and a photomultiplier. The solvent (ethanol) was partly removed by heating the gels with 5 mol.% and 10 mol.% of Eu^{3+} at 100 °C for 48 h. Powders with same concentration of Eu^{3+} were prepared from colloidal solutions by heating at 100, 150 and 200 °C for 48 h, and finally for 24 h at 300 °C or at 350 °C. The excitation pulse width was about 20 μs. The decays were simulated with a bi-exponential function $y_0 + A_1 \exp(-(t - x_0)/t_1) + A_2 \exp(-(t - x_0)/t_2)$.

3. Results and discussion

3.1. Eu,Ti@ZnO organosols

ZnO is a wide-bandgap (3.37 eV) semiconductor having a large exciton binding energy [13]. In its 'bulk' or 'nanosized' form, it can be used in a wide range of applications such as UV light emitters, gas sensors, transparent electronics and spintronic and surface acoustic wave devices [13, 14]. Recently, preparation of innovative functional ZnO nanomaterials by doping or functionalization of ZnO colloids (denoted here as @ZnO) has become a new challenge [12]. Even though this 'bottom up' approach has been known for more than 25 years [15], it is still debated, especially the very interesting and important topics of ZnO nanocrystals growth and ZnO by-products present in the nanocolloids [12, 16, 17]. Nevertheless, it is admitted that the simple sol–gel method yields nanocrystals which have the size of about 5 nm and emit a strong green–yellow luminescence under UV lamp as demonstrated in figure 1.

The exposure of ZnO nanocrystals to titanium alkoxide partially decomposes the ZnO nanocrystals, as demonstrated in our previous studies [18, 19], with the concomitant decrease in the hydrodynamic diameter to less than 3 nm [18]. This result was confirmed by XRD, UV-vis absorption, PL and DLS measurements [19]. Although the utilized sol–gel process resulted in a Ti@ZnO organosol which was stable over months, the viscosity of this organosol increased from 2.8 to 10 cP after a few days, resulting in the possible formation

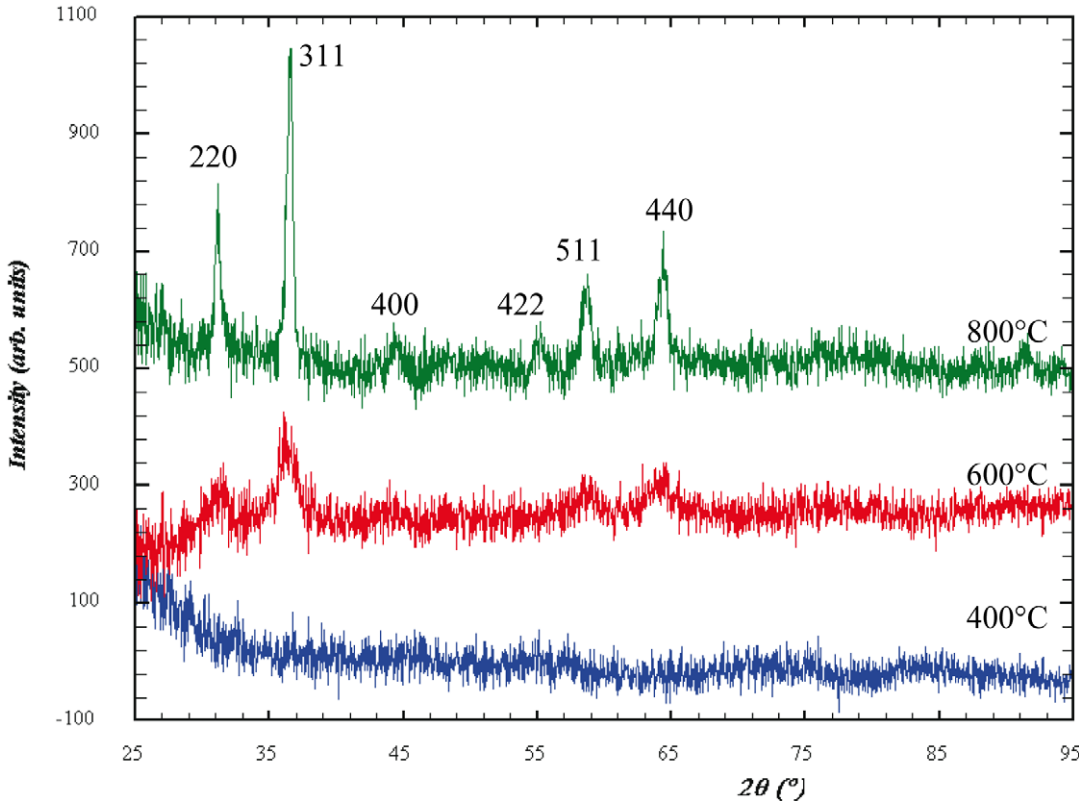

Figure 3. XRD patterns of a 'ZnTiO' thin film annealed at 400, 600 and 800 °C for 15 min in air (the silica substrate signal was removed).

of a transparent and luminescent xerogel [10]. All these results indicate strong modification of the starting @ZnO colloid with a transformation into a complex polymeric solution. Complementary Raman studies are being performed to elaborate these results.

As reported by Ashtaputre *et al* [20], the addition of Eu^{3+} does not drastically change the initial ZnO condensation process. The size of the ZnO nanoparticles was estimated at about 4 nm from the wavelength of the bandgap absorption edge and XRD patterns (see S1 and S2 in supporting information given in stacks. iop. org /STAM/11/. . . /mmedia). More important, however, is that the introduction of Eu^{3+} as a local probe and the study of the photoluminescence in Ti@ZnO organosols confirm the modification of the ZnO nanocrystals by the addition of titanium alkoxide. Indeed, after a few days the classical yellow luminescence of the ZnO organosol (figure 1) weakened revealing the red luminescence of europium. This is demonstrated in figure 2, which presents UV-excited visible luminescence from an organosol doped with 10% Eu^{3+}. The classical five emission peaks attributed to the $^5D_0 \rightarrow {}^7F_J$ transition of Eu^{3+} (where $J = 0, 1, 2, 3$ and 4) are observed with the strongest emission for $J = 2$ at 613 nm. The emission bands are inhomogeneously broadened owing to the site-to-site variation of Eu^{3+} properties. The maximum of intensity at the $^5D_0 \rightarrow {}^7F_2$ transition indicates the distorted nature of the sites. This hypersensitive transition is observed in the 600–635 nm range and provides information on the rare-earth site symmetry. Its strong intensity indicates that the local symmetry around the europium ions does not have the inversion center. This will be discussed in the next section dealing with optical properties of thin films.

3.2. Eu,Ti@ZnO thin films

Compounds in the $ZnO–TiO_2$ system are attractive catalysts and phosphors and are good regenerable sorbents for desulfurization of hot coal gases [21]. Zinc titanate h-$ZnTiO_3$ thin film is also a promising dielectric material for microwave devices and for low-temperature co-fired ceramics, owing to its relatively low sintering temperature and good dielectric properties [22–24]. There has been considerable interest in the chemical synthesis of these oxides, and it is well known that both zinc acetates and titanium alkoxides easily dissolve in such solvents as ethanol. For instance, the sol–gel synthesis and characterization of c-$ZnTiO_3$ thin films with perovskite structure using zinc acetate and titanium butoxide precursors were reported 10 years ago [25]. Both precursors were separately dissolved in dry ethanol, then mixed together and finally refluxed in N_2 atmosphere for 5 h to obtain a homogeneous spinable organic solution. More recently, we synthesized, for photocatalytic purpose, a new cation-deficient zinc titanium oxynitride with a spinel-type structure [3]. Using this simple and inexpensive @ZnO colloidal sol–gel route it was possible to prepare transparent and colored 1 micrometer thick 'ZnTiON' porous layers on silica.

In the experimental section above, we mentioned that with a simple doping process, a trivalent europium precursor could be easily introduced to the organosols, and that Ti@ZnO

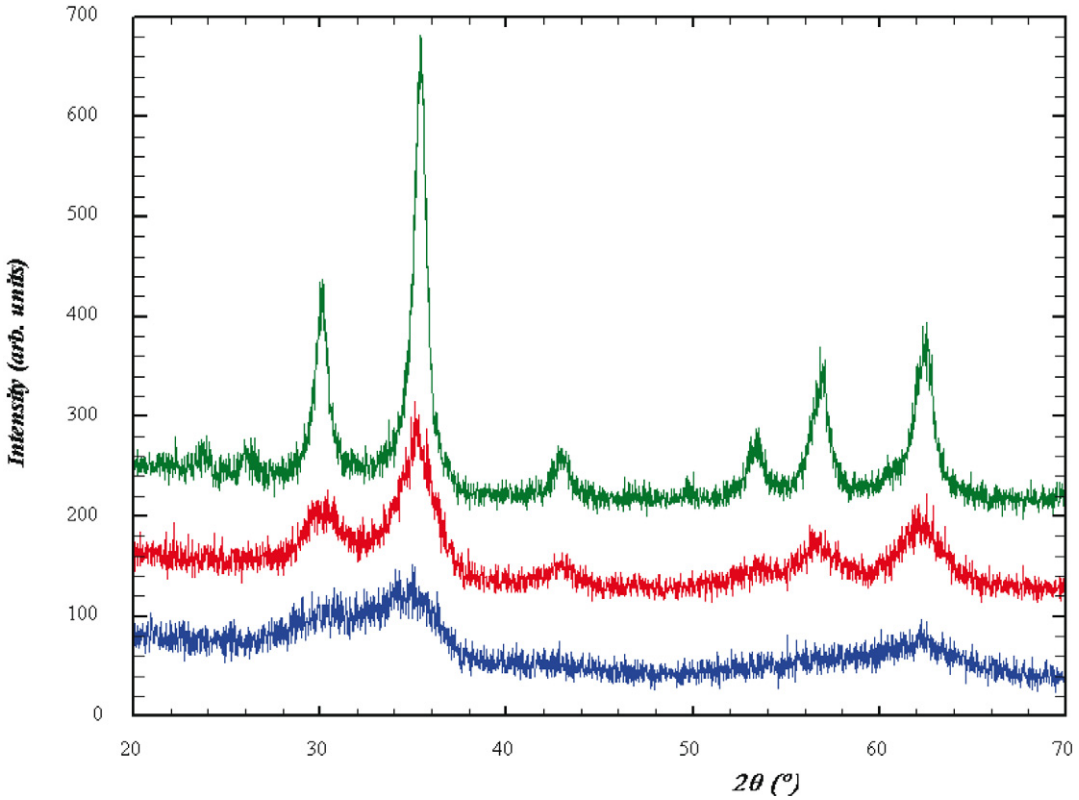

Figure 4. XRD patterns of a 'ZnTiO' xerogel annealed at 400, 500 and 600 °C for 24 h in air.

nanocrystals could therefore be used as nanohosts for Eu^{3+} cations. The wet films prepared from these Eu^{3+}, Ti^{4+}-@ZnO sols via dip-coating of glass slides were then pre-sintered at 400 °C for 15 min in air to remove the organic residues. The resulting layers were subsequently annealed in air for 15 min.

The Eu^{3+}-doped 'ZnTiO' films were further characterized by XRD to identify the crystalline phases formed at different temperatures. Figure 3 shows the patterns of the film annealed in air at 400, 600 or 800 °C for 15 min (the silica signal was subtracted). They were recorded at a low incident angle of 3° that increased the signal-to-noise ratio but also shifted the scattering angle [25].

In figures 3 and 4, distinct peaks can be detected only after annealing at 600 °C for 15 min in the case of thin films (figure 3) and 400 °C for 24 h in the case of xerogel nanopowders (figure 4). According to literature, several phases, including α-Zn_2TiO_4 (cubic, $Fd3m$) [26], h-$ZnTiO_3$ (hexagonal, $R\bar{3}$) [27], c-$ZnTiO_3$ (cubic) [28–30] or $Zn_2Ti_3O_8$ (cubic) [31] exist in the phase diagram of the ZnO–TiO_2 system. Whereas the first two phases are well identified and characterized, there are many contradictions for the last two cation-deficient spinel-type structures [31].

In our samples, all x-ray reflections can be indexed assuming a cubic cell ($a = 8.4$ Å), and the analysis of the room-temperature XRD data indicates that the 'ZnTiO' compound could be isostructural with the spinel-type structure α-Zn_2TiO_4 or a cation-deficient spinel-type structure like c-$ZnTiO_3$ or $Zn_2Ti_3O_8$. As demonstrated above and in table 1, according to the refined values of the lattice parameter and the chemical ratio between Zn and Ti (measured as 0.994 by EDX), it seems clear that the c-$ZnTiO_3$ structure could be stabilized between 400 and 800 °C. These results agree with those reported by Hosono *et al* [30]. Nevertheless, a stoichiometric mixture of α-Zn_2TiO_4 and $Zn_2Ti_3O_8$ could result in a similar chemical ratio and broad XRD peaks. Complementary Raman studies are in progress to better characterize these thin films.

Regarding the chemical stability of the xerogel powders, previous results obtained on a very similar material, using *in situ* XRD measurements while annealing in air, showed emergence of zinc oxide peaks between 150 and 450 °C for the Zn/Ti = 1 ratio. At higher temperatures (>700 °C), binary compounds such as cubic spinel were formed [19]. In this study, similar results were obtained for the Eu-doped 'ZnTiO' xerogel. In addition, extra phases like Eu_2TiO_5 were detected in the Eu–Ti–O system annealed at 800 °C. These results confirm that c-$ZnTiO_3$ is a metastable phase like h-$ZnTiO_3$ [30] and that the Eu^{3+} cation is not stabilized in the Zn–Ti–O phases at temperatures above 800 °C [9].

The microstructural properties of thin films were studied by SEM. Figure 5 shows the surface and cross section of a thin film obtained after two dips in a Eu^{3+}, Ti^{4+}-@ZnO colloidal solution. The film thickness could range from few tens of nanometers to 600 nm for one dip, depending on the dipping speed and viscosity of the solution, and the film surface was relatively smooth.

Figure 6 shows the optical transmission spectrum of the film presented in figure 5. The deposited layers have a high transparency even for thickness over one micrometer. A large optical bandgap value of ~3.9 eV was estimated from

Table 1. XRD signal intensities and angles 2θ for α-Zn_2TiO_4 and c-$ZnTiO_3$ (reference data) and our thin film and xerogel nanopowder samples.

α-Zn_2TiO_4 (JCPDS 25–1164) (a = 8.4602 Å, SG: $Fd3\,m$)		c-$ZnTiO_3$ (JCPDS 39–0190) (a = 8.4080 Å, SG: $P4132$)		Thin films annealed at 800 °C for 15 min		Xerogel powders annealed at 600 °C for 24 h	
2θ	Intensity	2θ	Intensity	2θ	Intensity	2θ	Intensity
		23.643	7	–	–	23.85	8
		25.956	6	–	–	26.11	8
29.827	35	30.033	45	30.10	60	29.96	40
		31.902	1	–	–	–	–
		33.679	2	–	–	–	–
35.136	100	35.380	100	35.52	100	35.31	100
36.742	4	38.576	2	–	–	–	–
42.717	13	42.995	9	43.11	9	42.83	9
		47.072	2	–	–	–	–
		49.642	3	–	–	49.79	2
52.978	11	53.345	15	53.25	8	53.31	13
		55.696	1	–	–	–	–
56.515	30	56.860	28	57.02	20	56.75	21
		59.137	2	–	–	–	–
		60.241	3	–	–	60.40	3
61.990	30	62.446	34	62.36	32	62.38	34
65.159	1			–	–	–	–

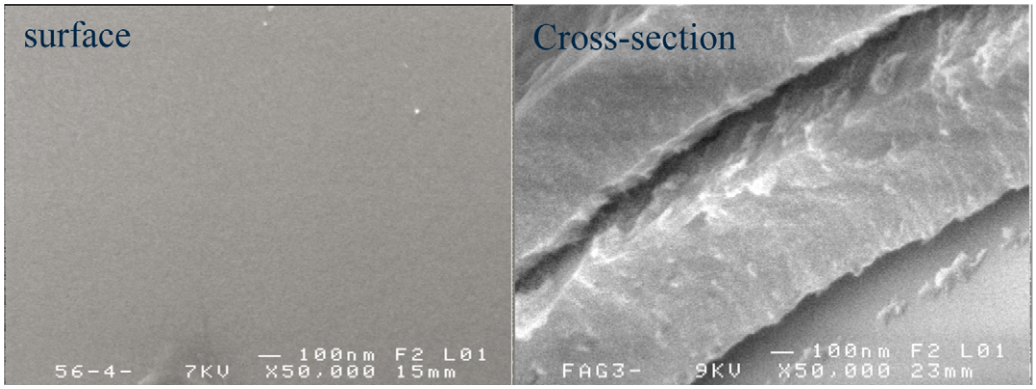

Figure 5. SEM images of a doped thin film annealed at 400 °C in air. Left: surface, right: cross section.

the plot of $(\alpha h\nu)^2$ versus. photon energy ($h\nu$) (see S3 in supporting information given in stacks. iop. org /STAM/11/ . . . /mmedia) and it agrees with the reported direct gap for c-$ZnTiO_3$ nanopowder [9]. The refractive index was measured on a single-dip thin film by ellipsometry, and the Cauchy dispersion relation was used for the data fitting (inset in figure 6). The refractive index varies between 1.73 and 1.63 in the wavelength range 400–1500 nm. The refractive index of a c-$ZnTiO_3$ thin film prepared by radio frequency reactive magnetron sputtering was previously measured by ellipsometry as ∼2.2 at 550 nm [21]. The lower value in our sample could be explained by the film porosity [4].

The red fluorescence of this new nanomaterial is easily observed at room temperature under 254 nm illumination from a compact 4W-UV lamp. It was possible to activate RE fluorescence in a highly transparent c-$ZnTiO_3$ thin film even after a relatively mild annealing at 400 °C for 15 min (figure 7).

In the studied spectral range of 560–660 nm, all films doped at 2.5, 5 and 10% of Eu show the characteristic emission of the intra-4f transitions ($^5D_0 \rightarrow {}^7F_0, {}^5D_0 \rightarrow {}^7F_1, {}^5D_0 \rightarrow {}^7F_2, {}^5D_0 \rightarrow {}^7F_3$) of Eu^{3+} ions centered at 578, 592, 613 and 653 nm, respectively (figure 8). The red luminescence corresponds to the transition $^5D_0 \rightarrow {}^7F_2$. The intensity ratios (noted R) of the transitions $^5D_0 \rightarrow {}^7F_2$ and $^5D_0 \rightarrow {}^7F_1$ are comparable with those recorded on the Ti@ZnO organosol doped with 10% of Eu^{3+}.

As observed previously [10], the majority of these films do not show sharp PL lines characteristic of Eu^{3+} in a bulk crystal, reflecting the presence of europium in an amorphous phase or in nanocrystals with the size below 10 nm [32]. The c-$ZnTiO_3$ nanocrystal growth could be hindered with the increasing Eu^{3+} content, likely due to the destabilizing effect of Eu^{3+} ions on the surface of a nanocrystal as reported for ZnO or TiO_2 nanocrystals [33, 34]. Moreover, Eu^{3+} ions could be located not only in the bulk but also at the surface lattice sites of the ZnO materials [32].

A continuous evolution of the shape of emission spectra with concentration of Eu^{3+} in our films could be expected, as observed for Eu^{3+}:TiO_2 mesoporous and dense films [35, 36]. At very low content of europium, its environment could be well defined, as in the bulk crystal. With the increasing Eu concentration in a nanocrystalline material, more and more Eu ions could be located at the surface that should broaden

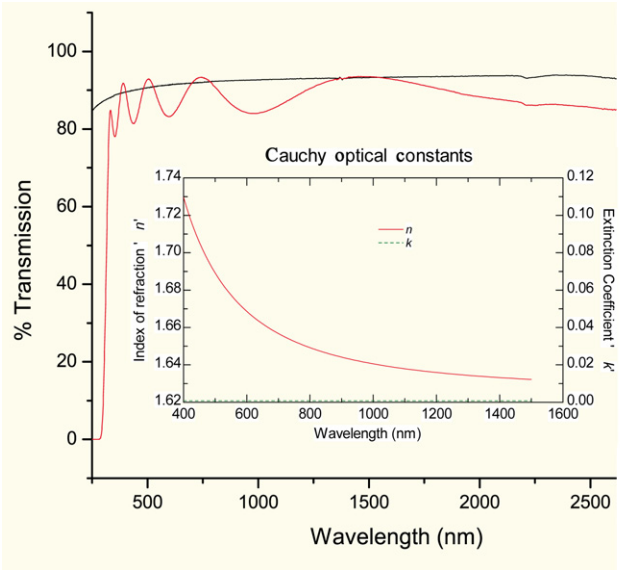

Figure 6. Optical transmission spectra of a thin 'ZnTiO' film annealed at 400 °C for 15 min (red line) and the silica substrate (black line). Inset: refractive index versus wavelength.

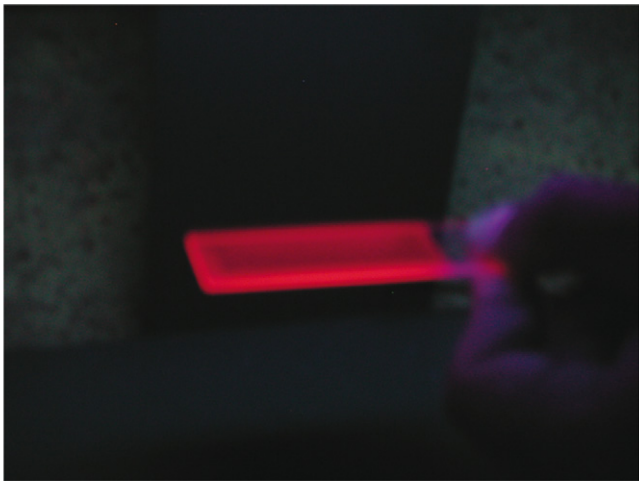

Figure 7. Eu^{3+} doped c-$ZnTiO_3$ thin film under UV illumination.

their emission lines. In this TiO_2–ZnO system annealed at 400 °C, the luminescence signals were broad for Eu^{3+} concentrations from 2.5 to 10%, as already reported for Eu^{3+}@TiO_2 nanocrystals [34]. This result reveals that the environment of a rare-earth element in TiO_2 nanomaterials is not as regular as in the bulk crystals, and a similar tendency could be observed in c-$ZnTiO_3$ nanocrystals. Broad emission signals are observed for the lowest studied concentration of Eu^{3+} for any annealing temperature used. Only the film doped with 5% of Eu^{3+} presents a marked peak sharpening upon annealing at 800 °C as compared to annealing at 400 °C (figure 8). Thus the annealed film with the Eu^{3+} concentration of 5% might include europium ions in a crystalline phase, such as Eu_2O_3 or Eu_2TiO_5.

The encouraging point is the strong $^5D_0 \rightarrow {}^7F_2$ emission resulting in red luminescence, in contrast to what is typically observed in orthoborate matrices ($TRBO_3$) doped with rare earth elements [8]. For borates YBO_3 and $ScBO_3$, which have

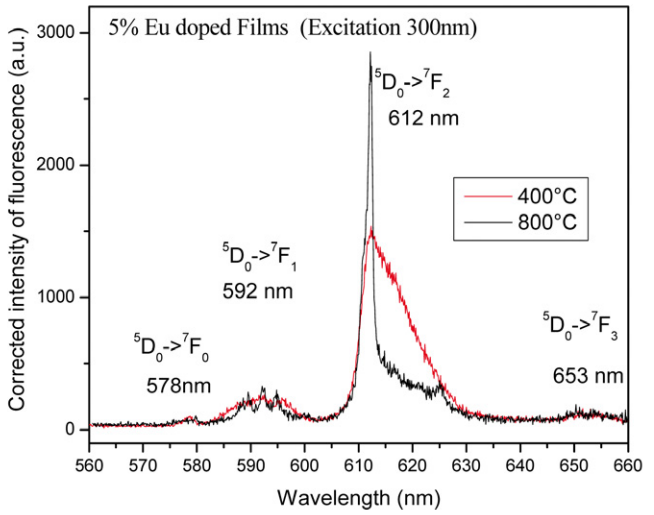

Figure 8. Luminescence spectra of 5% Eu^{3+} doped films annealed at 400 and 800 °C (300 nm excitation).

the inversion center in their lattice, the $^5D_0 \rightarrow {}^7F_1$ transition (magnetic dipole) is stronger than $^5D_0 \rightarrow {}^7F_2$ (electric dipole) resulting in an orange fluorescence with R values less than 1. This can be understood if one considers the site symmetry of europium. It is well accepted that the intensity ratio is a good indicator of the centrosymmetry in the Eu^{3+} environment [37, 38]. The effect of a non-centrosymmetric crystal field on Eu^{3+} ions is to lift the forbidenness of its electric dipole transitions. The $J = \pm 2$ transitions are hypersensitive to this effect, and even a small difference in the centrosymmetry of the site occupied by Eu^{3+} ions can make the usually weak magnetic dipole transitions dominant. The intensity ratio of the magnetic dipole and electric dipole transitions depends greatly on the crystalline structure. In these films, the ratio is about 6–8 (see figure 8). This is similar to the reported values (6–12) [39], indicating that Eu^{3+} ions are located at a low-symmetry site lacking the inversion center, whether they are in the well-crystallized phase, in amorphous phase or in a site characteristic of small nanoparticles. The low site symmetry is confirmed also by the three peaks in the region of the $^5D_0 \rightarrow {}^7F_1$ transition, indicating that the symmetry around the Eu^{3+} ions is lower than, e.g. C_{3v}.

A red shift and line narrowing are observed in the excitation spectra (figure 9), monitored at an emission wavelength of 613 nm ($^5D_0 \rightarrow {}^7F_2$ transition of Eu^{3+}), of the doped films annealed at different temperatures. The broad excitation band centered at 284 nm for the film annealed at 400 °C can be attributed to the bandgap excitation of the $ZnTiO_3$ matrix. Its presence in the excitation spectrum of Eu^{3+} emission suggests an energy transfer through defect states from the matrix to Eu^{3+} ions. The modification of excitation spectra upon annealing reveals the change in the Eu^{3+} environment from disordered to a more crystalline.

Figure 10 shows the decay of the 613 nm fluorescence ($^5D_0 \rightarrow {}^7F_2$ transition) in 5% Eu^{3+} doped Ti@ZnO powder and gel samples after room-temperature excitation at 300 nm. The decay is non-exponential, with a predominant short

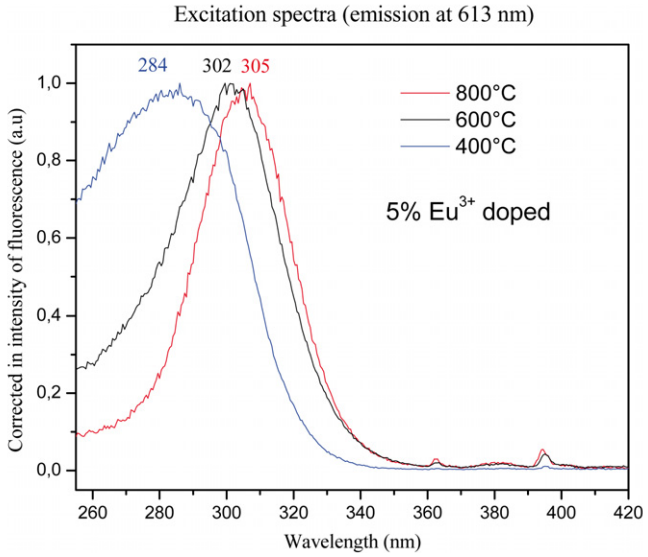

Figure 9. Excitation spectra of the 613 nm emission in the 5% Eu^{3+} doped films annealed at 400, 600 and 800 °C.

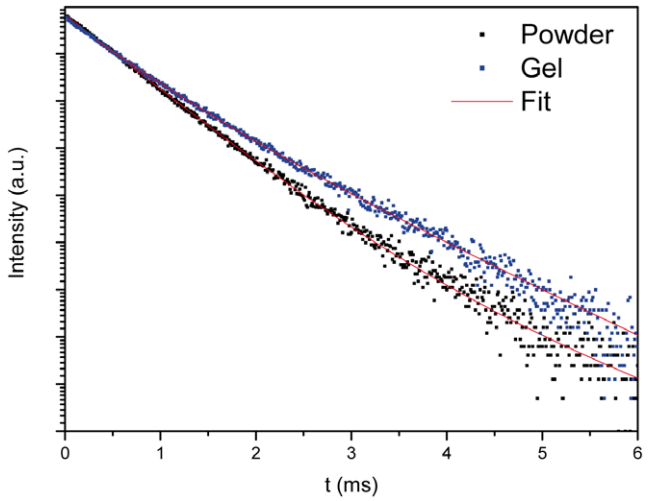

Figure 10. Fluorescence decays at 613 nm (300 nm excitation) in a 5% Eu^{3+} doped Ti@ZnO gel and powder.

lifetime of about 0.61 ms (±10%) and a longer component of 1.3 ms (±20%). The decay of the gel is faster, with the corresponding lifetimes of 0.57 and 1.04 ms. In ZnO nanocrystal, the corresponding lifetimes were 0.69 and 1.05 ms [33]. The multiexponential decay reveals that at least two kinds of Eu^{3+} centers coexist in the Ti@ZnO gel and powder. The shorter lifetime may be associated with europium at surface sites, where high concentrations of defects and impurities promote nonradiative relaxation, and the longer component may originate from europium at a regular crystal lattice site. Of course, a possible presence of europium oxide nanoparticles, which could be undetected by XRD or EDX because of the low signals, could also affect the reported lifetimes. Further experiments should be performed on this system at Eu concentrations below the solubility limit in the $ZnTiO_3$ matrix, avoiding the europium oxide nanoparticles and decreasing the contribution of the surface Eu^{3+}. Such experiments will result in a better understanding of the energy transfer between the matrix and Eu^{3+} levels.

4. Conclusion

To conclude, we prepared a novel, highly concentrated Eu^{3+}, Ti^{4+}@ZnO colloidal solution using a simple and inexpensive bottom-up process. We also demonstrated that this solution could be easily used to prepare functional transparent thin films, which show a strong red emission under UV illumination. c-$ZnTiO_3$ crystalline thin films can serve as a host matrix for Eu^{3+} cations and remain stable at temperatures up to 800 °C. This material can be fabricated in large enough slabs for applications in macroscopic products. We are planning to extend this approach to other systems such as Tb or Yb–Er functionalized Ti@ZnO materials.

Acknowledgments

The authors thank M J Le Lannic for supplying the SEM images and University of Rennes 1, University of Bordeaux, Region Bretagne, CNRS, ICMCB, YCIS and NIMS for financial support.

References

[1] Klabunde K J 2001 *Nanoscale Materials in Chemistry* (New York: Wiley-VCH)
[2] Sanchez C, Lebeau B, Chaput F and Boilot J P 2003 *Adv. Mater.* **15** 1969
[3] Grasset F, Starukh S, Spanhel L, Ababou-Girard S, Su D and Klein A 2005 *Adv. Mater.* **17** 294
[4] Pénard A-L, Gacoin T and Boilot J-P 2007 *Acc. Chem. Res.* **40** 895
[5] Camenzind A, Strobel R and Pratsinis S 2005 *Chem. Phys. Lett.* **415** 193
[6] Mansuy C, Tomasella E, Mahiou R, Gengembre L, Grimblot J and Nedelec J M 2006 *Thin Solid Films* **515** 666
[7] Chadeyron-Bertrand G, Boyer D, Dujardin C, Mansuy C and Mahiou R 2005 *Nucl. Instrum. Methods Phys. Res.* B **229** 232
[8] Jiang X C, Yan C H, Sun L D, Wei Z G and Liao C S 2003 *J. Solid State Chem.* **175** 245
[9] Mrazek J, Spanhel L, Chadeyron G and Matejec V 2009 *J. Phys. Chem.* C **114** 2843
[10] Grasset F *et al* 2008 *Int. J. Nanotechnol.* **5** 708
[11] Bahnemann D W, Kormann C and Hoffmann M R 1987 *J. Phys. Chem.* **91** 3789
[12] Spanhel L 2006 *J. Sol-Gel Sci. Technol.* **39** 7
[13] Pearton J, Norton D P, Ip K, Heo Y W and Steiner T 2005 *Prog. Mater. Sci.* **50** 293
[14] Vayssière L 2005 *Adv. Mater.* **15** 464
[15] Koch U, Fojtik A, Weller H and Henglein A 1985 *Chem. Phys. Lett.* **122** 5076
[16] Brois V, Giorgetti C, Dartyge E, Baudelet F, Tokumoto M S, Pulcinelli S H and Santilli C S 2006 *J. Sol-Gel. Sci. Techol.* **39** 25
[17] Grasset F, Sasaki T, Haneda H, Baudet C and Lavastre O 2008 *J. Colloid Interface. Sci* **317** 493
[18] Grasset F, Spanhel L and Ababou-Girard S 2005 *Superlattices. Microstruct.* **38** 300
[19] Berthebaud D, Grasset F, Allegret-Maret V, Ababou-Girard S and Pechev S 2007 *J. Phys. Chem.* C **111** 7883

[20] Ashtaputre S S, Nojima A, Marathe S K, Matsumura D, Ohta T, Tiwari R, Dey G K and Kulkarni S K 2008 *J. Phys. D: Appl. Phys.* **41** 015301
[21] Ye C, Pan S S, Teng X M, Fan H T and Lii G H 2008 *Appl. Phys.* A **90** 375
[22] Kim H T, Kim S H, Nahm S and Dyum J D 1999 *J. Am. Ceram. Soc.* **82** 1901
[23] Chaouchi A, d'Astorg S, Marinel S and Aliouat M 2007 *Mater. Chem. Phys.* **103** 106
[24] Deng Y, Lv Q, Wu S and Zhan S 2010 *Dalton Trans.* **39** 2497
[25] Phani A R and Santucci S 2001 *J. Mater. Sci. Lett.* **20** 573
[26] Rankin R B, Campos A, Tian H, Siriwardane R, Roy A, Spivey J J, Sholl D S and Johnson J K 2008 *J. Am. Ceram. Soc.* **91** 584
[27] Chai Y L, Chang Y S, Chen G J and Hsiao Y J 2008 *Mater. Res. Bull.* **43** 1066
[28] Yamaguchi O, Morini M, Kawabata H and Shimizu K 1987 *J. Am. Ceram. Soc.* **70** C97
[29] Li C, Bando Y, Nakamura M, Kimizuka N and Kito H 2000 *Mater. Res. Bull.* **35** 351
[30] Hosono E, Fujihara S, Onuki M and Kumira T 2004 *J. Am. Ceram. Soc.* **87** 1975
[31] Liu Z, Zhou D, Gong S and Li H 2009 *J. Alloys Compd.* **475** 840
[32] Mercier B, Dujardin C, Ledoux G, Louis C, Tillement O and Perriat P 2006 *J. Lumin.* **119–120** 224
[33] Liu Y S, Luo W Q, Li R F, Liu G K, Antonio M R and Chen X Y 2008 *J. Phys. Chem.* C **112** 686
[34] Zeng Q G, Ding Z J and Zhang Z M 2006 *J. Lumin.* **118** 301
[35] Leroy C M, Cardinal T, Jubera V, Treguer-Delapierre M, Backov R, Boissiere C, Grosso D, Sanchez C, Viana B and Pelle F 2009 *J. Lumin.* **129** 1641
[36] Sakaguchi I, Sato Y, Royken H, Hishita S, Ohashi N and Haneda H 2005 *Japan. J. Appl. Phys.* **44** 1289
[37] Judd B R 1962 *Phys. Rev.* **127** 750
[38] Ofelt G S 1962 *J. Chem. Phys.* **37** 511
[39] Leroy C M *et al* 2008 *ChemPhysChem* **9** 2077